The Onion-like Metallicity Structure of Tycho's Supernova Remnant as Revealed by Doppler Broadened X-ray Emission Lines

Asami Hayto[1,2], Toru Tamagawa[1], Hiroya Yamaguchi[1], Akihiro Furuzawa[3], Midori Ozawa[4],
Hideyo Kunieda[3], John P. Hughes[5], Una Hwang[6], Aya Bamba[7], Kazuo Makishima[8,1]

[1] RIKEN, [2] Tokyo University of Science, [3] Nagoya University, [4] Kyoto University,
[5] Rutgers University, [6] NASA/GSFC, [7] ISAS/JAXA , [8] University of Tokyo
E-mail(AH): hayato@crab.riken.jp

ABSTRACT

We have discovered a three-dimensional onion-like metallicity structure in Tycho's SNR using *Suzaku*, in such a way that iron is more concentrated in the remnant center than intermediate-mass elements (IMEs: Si, S, Ar, and Ca). This is achieved by measuring widths of the emission lines of those elements as a function of the angular distance from the center of the remnant. We interpret our results as representing Doppler broadening caused by a line-of-sight velocity dispersion of the line-emitting ions. Applying two Gaussian models (red- and blue-shifted components) to each broadened line, we determine the expansion velocities of the IMEs and Fe as $\sim$4900 km s^{-1} and $\sim$3800 km s^{-1}, respectively. Combining our results with the projected image of the SNR, we successfully construct a three-dimensional onion-like structure of the SNR.

KEY WORDS: ISM: supernova remnants — supernovae: general — X-rays: individual (Tycho's SNR)

1. Introduction

Type Ia supernovae (SNe) play a key role as cosmological probes or tracers for the chemical evolution of galaxies. In spite of their importance, our knowledge of physical mechanisms of explosion has been incomplete. X-ray emission from ejecta in young supernova remnants (SNRs) should include evidence of progenitors and explosions. For example, distribution of materials in the remnants might reflect the structure of products by the SN explosion. Tycho's SNR originates in the SN in 1572, and is confidently classified as a Type Ia SNR in several ways. Because of the known age, simple morphology, and clear type determination, it has been an ideal target for a study of Type Ia SNRs.

The past X-ray observations (e.g., Hwang & Gotthelf 1997, Hwang et al. 1998, Decourchelle et al. 2005) reveled that Fe-Kα emitting ejecta are likely situated somewhat inner comparing to the intermediate-mass elements (IMEs, e.g., Si, S, Ar, and Ca). In SN 1006 (Yamaguchi et al. 2008) and SNR 0509-67.5 (Kosenko et al. 2008), which are also categorized Type Ia SNRs, the same situations have been reported.

Furuzawa et al. (2009) found that the Fe Kα line is significantly broadened at the center of the remnant using the data obtained by *Suzaku*. They discussed that it is likely because of the Doppler effect by the shell expansion with the velocity of $\sim$3000 km s^{-1}. We extend their

analysis to the lines of IMEs as well, and measure the velocity of ejecta in each element, so that we can construct the three-dimensional structure of materials in Tycho's SNR.
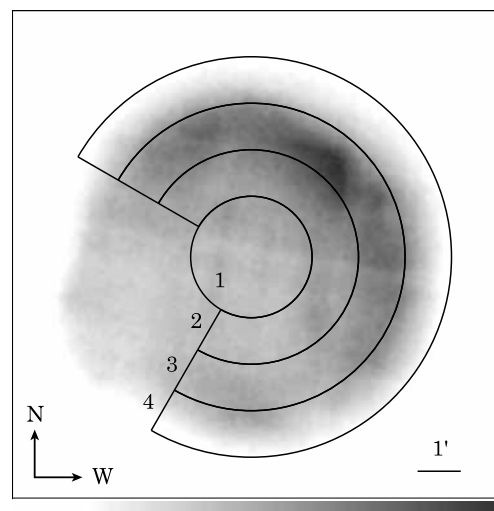

Fig. 1. XIS image of Tycho's SNR.

2. Observation

Suzaku observed Tycho's SNR and its off-source background on 2006 June 26-29 and 29-30, respectively, as

a part of the scientific working group time. After data screening, the left effective exposure was 101 ksec.

3. Spatially Resolved Spectra

The XIS FI image of the SNR is shown in Figure 1. In order to measure the centroid energies and line widths of lines as a function of the remnant position, we divide the SNR into 4 radial region, as also shown in Figure 1, numbered from 1 (inner) to 4 (outer). We exclude the southeast region where the irregular clumps are situated. The background spectrum is taken from the offset observation.

3.1. Spectral Fitting

We analyze the spectrum of each region in two representative energy bands separately to reduce the parameters of fitting: the $1.7-5$ keV for the lines of IMEs and the $5-8$ keV for the Fe-K lines.

The model we apply to the $1.7-5$ keV spectrum in each region (the single Gaussian model hereafter) includes an absorbed power-law and 20 Gaussian components: Heα, Heβ, Heγ, Lyα, and Lyβ ($n = 2 \rightarrow 1, 1s3p \rightarrow 1s^2$, and $1s4p \rightarrow 1s^2$ transition in He-like ion, and $n = 2 \rightarrow 1$ and $3p \rightarrow 1s$ transition in H-like ion, respectively) emission lines of Si, S, Ar, and Ca. All Gaussian parameters for the well-resolved lines, i.e., Heα of Si, S, Ar, and Ca, and Heβ lines of Si and S, are left free, while parameters of other lines are set based on the feasible assumption of non-equilibrium plasma with electron temperature kT_e and ionization timescale $n_e t$ of ~ 1 keV and $\sim 10^{11}$ cm^{-3} s (Hwang & Gotthelf 1997), respectively. We fit the $5-8$ keV spectra of each region with a power-law and three Gaussian lines representing the Kα blends of low ionized Fe and Ca, as well as the Kβ line of Fe. All parameters are allowed to vary freely, but the widths of Cr Kα and Fe Kβ lines are tied to that of the Fe Kα. Figure 2 represents the spectra of region 3 with the best-fit single Gaussian models. We obtain good fits for all spectra for region $1-4$.

3.2. Radial Line Profiles

Figure 3 shows the radial line profiles of IMEs and Fe, obtained in the previous section. The centroid energies of all elements, except Ca, are constant with radius. By contrast, the widths significantly decrease from the center to the rim. We note that the systematic uncertainties due to the intrachip gain variation across the remnant is $\pm 0.2\%$, which are also shown in Figure 3.

In order to explain those variations of the centroid energies and widths, we consider a spherically-symmetric shell expansion of the remnant. In this case, the emission lines from retreating and approaching shells to the observer should be red- and blue-shifted, respectively. Therefore, the lines at the center of the SNR should be
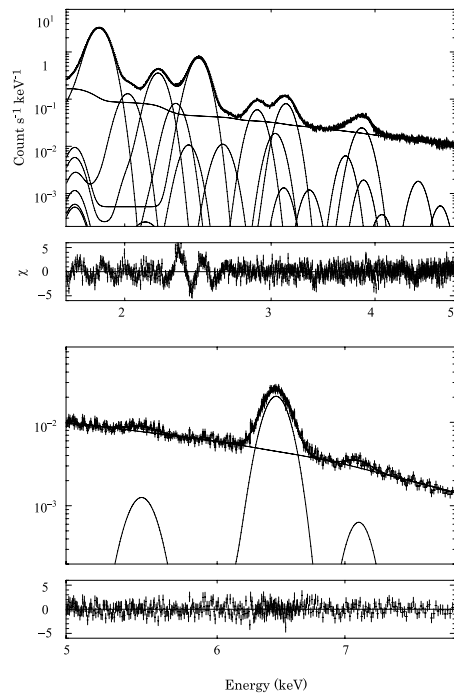

Fig. 2. Spectra of region 3 with the best-fit single Gaussian fit model in $1.7-5$ keV (left) $5-8$ keV (right) bands.

broader than that at the rim where the less line-of-sight velocity would be observed.

4. Analysis with Shell Expansion Model

Considering the spherically-symmetric shell expansion, a broadened line at the center of the remnant should be composed of red- and blue-shifted lines. We thus can derive the velocities of the ejecta from the differences of the centroid energies between both components.

4.1. Spectral Fitting

In this analysis, we take the spectrum of region 1 where the line-of-sight velocity should be maximized. Again, we fit the spectra in two energy bands separately. We here assume that each broadened line consists of the red- and blue-shifted lines, and thus the model includes a power-law and 40 Gaussian lines (the double Gaussian model hereafter). The widths of all Gaussian models are fixed to those expected from the single non-equilibrium collisional plasma model version 1.1 in XSPEC: 10, 13, 17 and 50 eV for Heα of Si, S, Ar, and Ca lines, respectively. Line intensities of red- and blue-shifted pairs are linked with each other, and those intensities are treated in the same way as the single Gaussian model. Centroid energies of both red- and blue-shifted lines of all Heα lines are left free parameters. In the $5-8$ keV spectra, we also apply the double Gaussian model to the Fe Kα line. The fixed width is 35 eV, by assuming a single
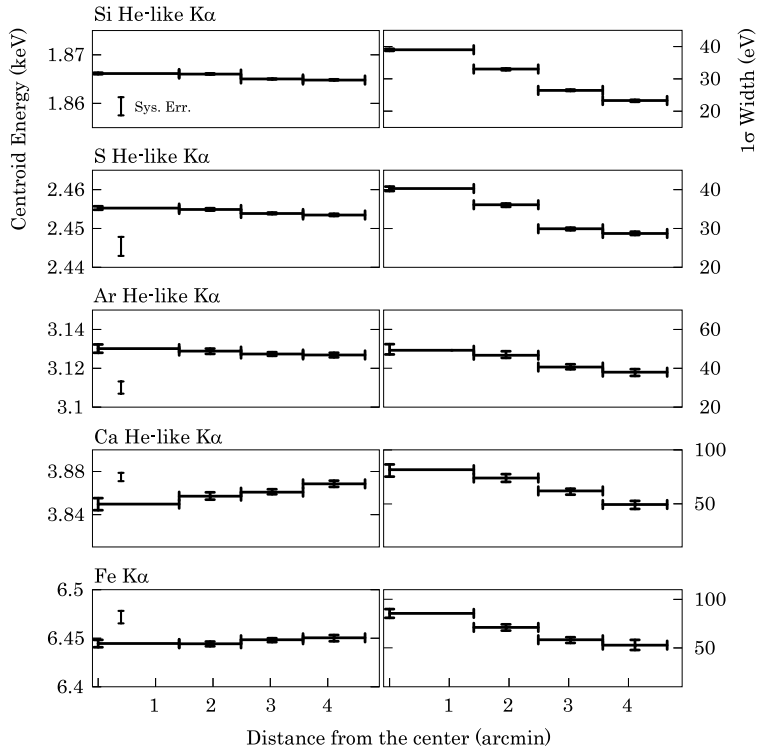
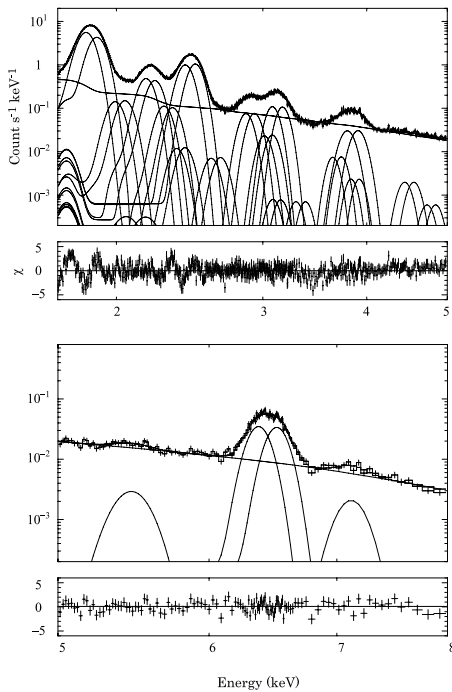Fig. 3. Radial line profile of Heα of Si S, Ar, and Ca, and Fe Kα lines.

Fig. 4. Spectra of region 1 with the best-fit double Gaussian fit model in 1.7−5 keV (left) 5−8 keV (right) bands.

ionization state (Furuzawa et al. 2009), and the intensities of two lines are tied with each other. The centroid energies of both lines are free parameters. We obtain the good fits both for 1.7−5 keV and 5−8 keV spectra. The spectra with the best-fit double Gaussian models are shown in Figure 4.

4.2. Expansion Velocity

We then convert the centroid energy difference between the red- and blue-shifted lines into expansion velocity by an equation of non-relativistic Doppler effect,

$$\frac{1}{2}\frac{\delta E}{E_0} = \frac{v_\perp}{c}, \tag{1}$$

where the δE, E_0, and $v_\perp$ are a centroid energy difference between the red- and blue-shifted components, rest-frame energy, and a line-of-sight velocity, respectively. Here, we need some correction. First, the line-of-sight velocity seen from the observer is continuously decreasing from the center to the rim. We thus calculate the mean line-of-sight velocity we would observe in region 1, which is 0.86 v_{exp}, where v_{exp} is an actual expansion velocity. Second, due to the smearing effect of the XRT (the half power diameter of 2′), only 48% of observed events in region 1 originate from this sky region, and other events actually come mainly from region 2 and 3 (See Furuzawa et al. 2009 in detail). Combining this

Table 1. Centroid energy difference and velocity

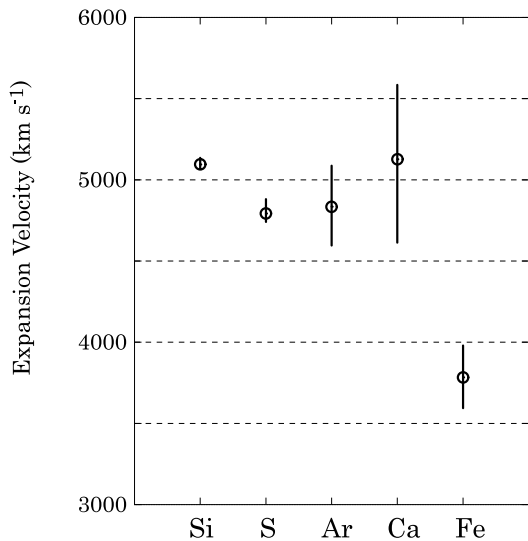|	δE (eV)	Velocity (km s^{-1})
Si	$55.1^{+0.4}_{-0.3}$	5090^{+40}_{-30}
S	$68.2^{+1.3}_{-0.7}$	4300^{+100}_{-200}
Ar	88^{+5}_{-4}	4800^{+300}_{-200}
Ca	110 ± 10	5100 ± 500
Fe	142 ± 7	3800 ± 200

Fig. 5. Expansion velocity of ejecta.

smearing effect with the mean line-of-sight velocity, actual $v_\perp$ we would observe in region 1 is estimated as 0.87 $v_{\exp}$. As the results, the translated expansion velocities are summarized in Table 1 and Figure 5. We found that IMEs have significantly higher velocities than Fe Kα emitter. We should note that the Ca Heα line might be broadened by not only the shell expansion but also the multi-ionization ages effect, since the centroid energy of this line is significantly increasing from the center to the rim. In this analysis, however, we cannot discriminate those effects. To investigate more accurate velocity of Ca, a feature observation with higher energy resolution is required.

5. Discussion
5.1. Distribution of Matter
Image analysis of past X-ray observations, e.g., Hwang & Gotthelf (1997), Decourchelle et al. (2001), and Warren et al. (2005), implied that the Fe-K emitter are concentrated in the center compared from the other lighter elements. This work reveals the three-dimensional onion-like structure of ejecta, inlaying Fe-K emitting ejecta and outward IMEs. This stratification agrees with a picture where the heavier elements are synthesized at deeper layer of the progenitor (Iwamoto et al. 1999).

5.2. Distance to Tycho's SNR
Our results of ejecta velocity are completely independent from the distance. Recent work of Katuda et al. (2009) measured the proper motions of ejecta μ from *Chandra*'s $1-8$ keV band images taken in 2000, 2003, and 2007. Combining the velocity with their result, we can estimate the distance to the target. Using the velocity of Si, of which emission is dominant in this energy band, we drive the distance of 4.1 ± 1.2 $(v/4900$ km s$^{-1})(\mu/0.253$ yr$^{-1})^{-1}$ kpc. The error represented above is dominated by the azimuthal variation of μ. This result well agrees with the distance determined in several independent ways, e.g., the proper motion of the optical filament and shock velocity ($1.9-3.3$ kpc; Ghavamian et al. 2001), the observation of HI absorption (4.6 ± 0.5 kpc; Schwarz et al. 1995), and comparing the historical record of SN peak luminosity with the absolute peak luminosity of Type Ia SNe ($3.8^{+1.5}_{-1.1}$ kpc; Krause et al. 2008).

References
Decourchelle, A. et al. 2001 A&A., 365, L218
Furuzawa, A. et al. 2009 ApJ, 693, L61
Ghavamian, P. et al. 2001 ApJ., 547, 995
Hwang, U & Gotthelf, E. V. 1997 ApJ., 475, 665
Hwang, U. et al. 1998 ApJ., 497, 833
Iwamoto, K. et al. 1999 ApJS., 125, 439
Katuda, S. et al. ApJ., submitted
Kosenko, D. et al. 2008 A&A., 490, 223
Krause, O. et al. 2008 Nature, 456, 617
Schwarz, U. J. et al. 1995 A&A., 229, 193S
Warren, J. S. et al. 2005 ApJ., 634, 376
Yamaguchi, H. et al. 2008 PASJ., 60, S141